Electronic structure and localization properties of $C_{60}Ta_n$ clusters ($n=1,3$): A first-principles study

Masahiko Matsubara,[1] Carlo Massobrio,[2] Lavanya M. Ramaniah,[3] Eliseo Ruiz,[4] and Mauro Boero[2,5,6]

[1]*Laboratoire de Physique des Matériaux, University of Poitiers, UFR Sciences SP2MI, Boulevard Marie et Pierre Curie, BP 30179, 86 962 Futuroscope Chasseneuil, France*

[2]*Institut de Physique et Chimie des Matériaux de Strasbourg (IPCMS), UMR 7504, CNRS-UdS, 23 Rue de Loess, F-67037 Strasbourg, France*

[3]*Synchrotron Radiation Section, Physics Group, Bhabha Atomic Research Centre, Trombay, Mumbai 400085, India*

[4]*Departament de Química Inorgànica and Centre Especial de Recerca en Química Teòrica (CeRQT), Universitat de Barcelona, Diagonal 647, 08028 Barcelona, Spain*

[5]*JAIST, 1-1 Asahidai, Nomi-shi, Ishikawa 923-1292, Japan*

[6]*CREST, Japan Science and Technology Agency, Sanban-cho, 102-0075 Tokyo, Japan*

(Received 12 October 2009; revised manuscript received 3 May 2010; published 25 May 2010)

The electronic structure and the electronic localization properties of the exohedrally doped fullerene $C_{60}Ta$, $C_{60}Ta_2$, and $C_{60}Ta_3$ systems are studied in the framework of density functional theory calculations. The effect of doping the fullerene network with Ta impurities results in modifications of the Kohn–Sham energy levels spectrum in the highest occupied molecular orbital–lowest unoccupied molecular orbital (HOMO-LUMO) region and a drastic HOMO-LUMO band-gap reduction. In the vicinity of the HOMO, most of the occupied electronic states are Ta-like for $C_{60}Ta$ and $C_{60}Ta_2$, while C-like states or mixed C-Ta-like states are predominant for the case of $C_{60}Ta_3$. In all cases, we observe a conspicuous charge transfer from the Ta to the neighboring C atoms, Mulliken charges are positive on the Ta atoms and equal to 2.12 ($C_{60}Ta$), 1.77/1.80 ($C_{60}Ta_2$), and 1.61/1.62 ($C_{60}Ta_3$). The values of the valence charges on the Ta atoms reflect their coordination environment and are the largest in $C_{60}Ta_3$ (3.00/3.25). This is compatible with the existence of three nearest neighbors (two Ta and one C) for each one of the Ta atoms in $C_{60}Ta_3$. We provide an insight into the physical nature of bonding by means of an accurate electronic structure analysis in terms of the electron localization function and the maximally localized Wannier orbitals. Among the Ta valence electrons, the most localized ones are those not involved in bond formation, charge transfer effects concurring to the establishment of ionic-covalent bonds between the Ta and the neighboring C atoms.

DOI: 10.1103/PhysRevB.81.195433 PACS number(s): 71.15.Pd, 32.10.Dk, 61.25.Em

I. INTRODUCTION

Transition metal (TM) atoms can act as dopant species altering the chemical nature of fullerenes, as proved by the synthesis and detection of endohedral, exohedral, and substitutional heterofullerenes.[1,2] In these three classes of systems, TM atoms play the role of foreign impurities interacting with carbon atoms assembled in a cagelike fashion. As a theoretical counterpart to experiments, density-functional theory (DFT) provides a well-suited and reliable approach to elucidate the relationship between the bonding properties of the fullerenes and the nature of the dopants.[3] However, while several studies of TM substitutional and endohedral heterofullerenes have been reported over the years,[4–12] the literature about the electronic structure of exohedral TM is nearly nonexistent.[11,13] The main purpose of this paper is to fill this gap by describing the electronic properties of Ta-doped exohedral heterofullerenes.

We take advantage of an available structural study carried out at the DFT level[13] to gain insight into the bonding features of $C_{60}Ta$, $C_{60}Ta_2$, and $C_{60}Ta_3$. We elucidate fundamental issues such as the charge state of the dopant atoms and of their nearest neighbors, their valence character, and the localization of the valence electron density in the vicinity of the dopant sites. For both experiments and theory, the case of $C_{60}Ta_x$ clusters has proved particularly challenging. According to mass spectrometric studies, fragmentation of the pristine $C_{60}Ta_x$ species goes along with the loss of C_3 units upon laser irradiation.[14] Motivated by this intriguing fragmentation behavior, the determination of the structure of $C_{60}Ta$, $C_{60}Ta_2$, and $C_{60}Ta_3$ heterofullerenes and the study of their dynamical evolution were achieved in the framework of first-principles molecular dynamics.[13] This has led to an accurate structural description of the most stable isomers and to a picture of the Ta mobility on the cage surface. To complete the atomic-scale characterization of these systems, we provide in this work detailed information on the electronic structure of $C_{60}Ta$, $C_{60}Ta_2$, and $C_{60}Ta_3$. This allows us to rationalize the interplay between the topology of these clusters and the bonding properties.

The scenario depicted by our results can be summarized in a clear evidence for a bonding character of the Ta atoms which is dependent on the local environment. An analysis of the electronic localization confirms that in $C_{60}Ta$ and in $C_{60}Ta_2$, no more than two electrons on each Ta atom (electronic configuration $[Xe]4f^{14}5d^36s^2$) are available for direct bonding with neighboring Ta or C atoms. Ta becomes trivalent in $C_{60}Ta_3$ by making available three valence electrons involved in two Ta-Ta bonds and one Ta-C bond.

The present paper is organized as follows. Our methodology is presented in Sec. II. It contains a summary of the computational framework, with an explicit account of the

electronic localization tools employed in this work. In Sec. III, we focus on the electronic properties of $C_{60}Ta$, $C_{60}Ta_2$, and $C_{60}Ta_3$. The indications collected by relying on the Kohn-Sham orbitals and the population analysis are completed and substantiated via a study of the electronic localization (electronic localization function, ELF, and Wannier functions, WF). Finally, concluding remarks are presented in Sec. IV.

II. COMPUTATIONAL METHODOLOGY

The theoretical framework and its implementation are identical to the one already used in the previous investigation devoted to the structural and dynamical properties of $C_{60}Ta$, $C_{60}Ta_2$, and $C_{60}Ta_3$ heterofullerenes.[13] Here, we recall that the calculations are performed via first-principles molecular dynamics.[15,16] This approach is based on DFT with gradient corrections after Becke (B) (Ref. 17) and Lee, Yang, and Parr (LYP) (Ref. 18) for the exchange and correlation functionals, respectively. A plane-wave basis set is used to represent valence electrons, with an energy cutoff of 70 Ry, and the core-valence interactions are described by Trouiller-Martins norm-conserving pseudopotentials.[19]

For computational convenience, the search of the optimized structures was repeated by placing the clusters in a face-centered cubic simulation cell with an edge of 26.46 Å, amounting to 4 times the diameter of the C_{60}. The structural features of the isomers were found very close to those reported in Ref. 13, to which we refer for a detailed description of the method and of the clusters configurations thereby obtained.

The electronic structure of the various heterofullerenes was first investigated by an analysis of the Kohn-Sham (KS) energy levels and of the associated probability density distributions of the electronic states, focusing on those around the highest occupied molecular orbital (HOMO)–lowest unoccupied molecular orbital (LUMO) energy gap. A population analysis was then performed to yield, for each atom, Mulliken charges and the valences. A deeper insight of the bonding localization properties can be achieved by the formalism of the ELF (Refs. 20–23) and of the Boys localized orbitals.[24] The ELF is defined as

$$\eta = \frac{1}{1+\chi^2}, \tag{1}$$

where

$$\chi = \frac{\sum_i |\nabla \psi_i|^2 - \frac{(\nabla \rho)^2}{4\rho}}{\frac{3}{5}(6\pi^2)^{2/3}\rho^{5/3}}. \tag{2}$$

Since we use a supercell approach, the Boys localized orbitals are calculated as their periodic system generalization, namely, the maximally localized WFs (Refs. 25 and 26) and the weighted center of their charge distribution, i.e., the Wannier function centers (WFCs).

The ELF provides information on the degree of localization of the electronic density.[27,28] By decreasing the ELF values from 1 (low-Pauli repulsion, highest localization), one can identify regions in space (termed *attractors*) which are surrounded by disjoint ELF isosurfaces (the basins) defining different charge localization domains. On lowering the ELF values, different degrees of localization can be established, not necessarily all related to bonding formation, as shown in a revealing example for the case of $C_{59}Si$.[29,30] In that case, the first localization domain on lowering the ELF appeared above the dopant Si atom and not along the Si-C bonds, clearly demonstrating that the ELF analysis can be more insightful than the conventional observation of the valence charge density.

Inspections in terms of localized orbitals were performed by computing the WFs and WFCs. Namely, WFs are obtained by a unitary transformation of the occupied Bloch orbitals. It should be recalled that, in principle, the WFs are not uniquely defined due to the arbitrary phase factor of the Bloch orbitals. This indeterminacy has been resolved in Ref. 26 by requiring that the total spread of the Wannier functions

$$S = \sum_n (\langle r^2 \rangle_n - \langle \mathbf{r} \rangle_n^2) \tag{3}$$

be minimized in real space.

III. ELECTRONIC PROPERTIES

A. Kohn-Sham orbitals

We carried out the study of the electronic properties by focusing on the most stable isomers of $C_{60}Ta$, $C_{60}Ta_2$, and $C_{60}Ta_3$, respectively.[13] In what follows, we refer to these specific isomers when invoking $C_{60}Ta$, $C_{60}Ta_2$, or $C_{60}Ta_3$. When describing the Kohn–Sham energy levels, the zero of the energy is taken as the highest occupied state between the two uppermost majority and minority spin levels. We recall that the nominal valence number of Ta is 5 and the related electronic configuration of this atom is $[Xe]4f^{14}5d^36s^2$. Since we work in a spin-unrestricted local spin density (LSD) approach, minority and majority spin states, labeled as α and β, respectively, are kept separated in the figures.

To get an insight into the localized character of the orbitals, each Kohn-Sham energy level is projected onto atomic orbitals centered on given atoms. In particular, this proves useful for the eigenstates around the band gap, since these states are generally expected to be the most affected by chemical reactions such as the formation of new Ta-C chemical bonds. Eigenstates characterized by close proportions of Ta and C characters are labeled as having a mixed Ta-C nature.

The fivefold degeneracy of the HOMO level and the threefold degeneracy of the LUMO level of the bare C_{60} are removed because of the presence of the Ta atom (case of $C_{60}Ta$, Fig. 1). Taking into account the spin and the presence of a Ta atom, 15 orbitals are expected to appear around the HOMO location. Indeed, seven α states appear, in the range between −0.77 and −0.03 eV. Three of these states are mostly Ta-like, whereas the other four, three mostly C-like and one having a mixed Ta-C nature, arise from the degeneracy removal of the HOMO level of C_{60}. A similar scenario

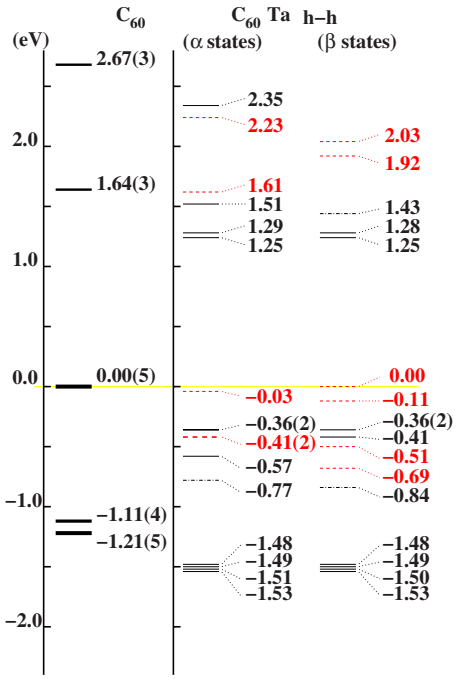

FIG. 1. (Color online) Kohn-Sham eigenvalues close to the band gap for C_{60} and for the most stable isomer of $C_{60}Ta$. The numbers in the parentheses denote the degeneracy of the energy levels. Solid and dashed lines indicate levels with a dominant C-like and Ta-like characters, respectively. Dash-dotted lines indicated mixed Ta-C levels.

holds also for the β states, where among the eight levels distributed between 0 and −0.84 eV, four are predominantly Ta-like. This description is complemented by the visual inspection of the associated $|\psi_i(\mathbf{x})|^2$ KS eigenstates for the orbitals corresponding to the HOMO-1, HOMO, and LUMO levels of $C_{60}Ta$ (Fig. 2). The HOMO state of the α-spin band is mainly localized around the Ta atom and, in particular,

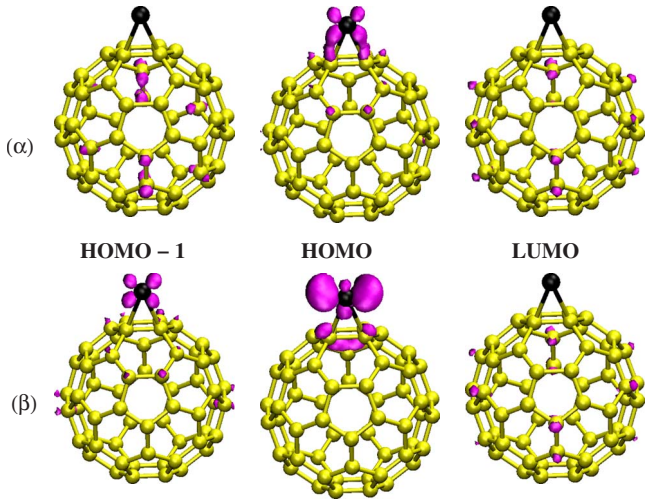

FIG. 2. (Color online) The probability isodensity surfaces, taken at the value 0.005 $e/(a.u.)^3$, for the eigenstates HOMO-1, HOMO, and LUMO of the most stable isomer ($h-h$) of $C_{60}Ta$. Top row for the α (minority) spin states and bottom row for the β (majority) spin states.

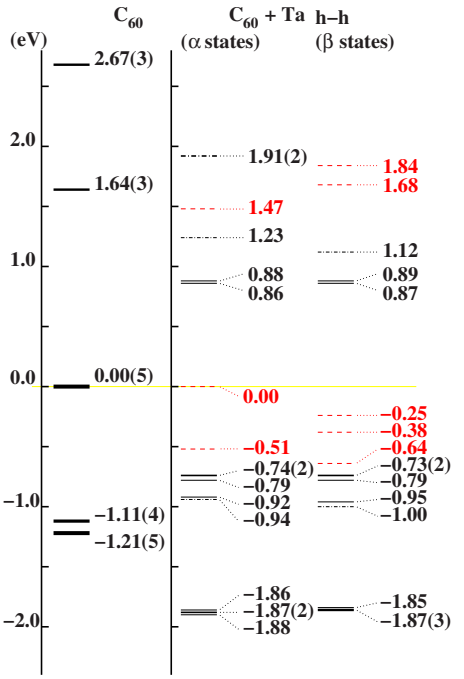

FIG. 3. (Color online) Kohn-Sham eigenvalues close to the band gap for C_{60} and for the unrelaxed isomer of $C_{60}Ta$. This has been obtained (see text) by keeping frozen the coordinates of C_{60} and by positioning the Ta atom at the location and distance from the C_{60} cage found in the relaxed case. The numbers in the parentheses denote the degeneracy of the energy levels. Solid and dashed lines indicate levels with a dominant C-like and Ta-like characters, respectively. Dash-dotted lines indicated mixed Ta-C levels.

along the Ta-C bonds. Similarly, in the case of the HOMO β-spin state, a nonnegligible weight along the $h-h$ bond has been evidenced (note that by $h-h$ bond we intend one of the hexagon-hexagon bonds of the C_{60} cage). On the other hand, the LUMO states of both α and β spin components are localized on regions of the fullerene distant from the Ta atoms. The HOMO-1 and LUMO of the α spin component are mostly carbonlike states and are separated by $\Delta E = 1.61$ eV, which is close to the HOMO-LUMO gap of C_{60} (1.64 eV). This is true also in the case of the β spin component when considering the states HOMO-2 and LUMO, having a carbonlike character and being separated by an identical energy difference (1.61 eV), whereas the HOMO-1 state of the β band is mainly Ta-like.

In Fig. 3, we show the Kohn-Sham energy levels of a C_{60}+Ta system in which the C_{60} is left unrelaxed. The position and the distance with respect to the underlying C_{60} network are taken to be those pertaining to the above C_{60}+Ta case. The constraint on the structure of the cage is reflected by the existence of fairly large residual energy gap between the HOMO and HOMO-1 eigenstates in the α spin band (0.51 eV), whereas as smaller gap (0.13 eV) is present in the β spin band. Also, distinct sets of Ta-like eigenstates and C-like eigenstates are found well separated around the HOMO level, underscoring a reduced hybridization with respect to the relaxed $C_{60}Ta$ case.

The Kohn-Sham energy levels of $C_{60}Ta_2$ are shown in Fig. 4. The majority of the orbitals located between 1.74 and

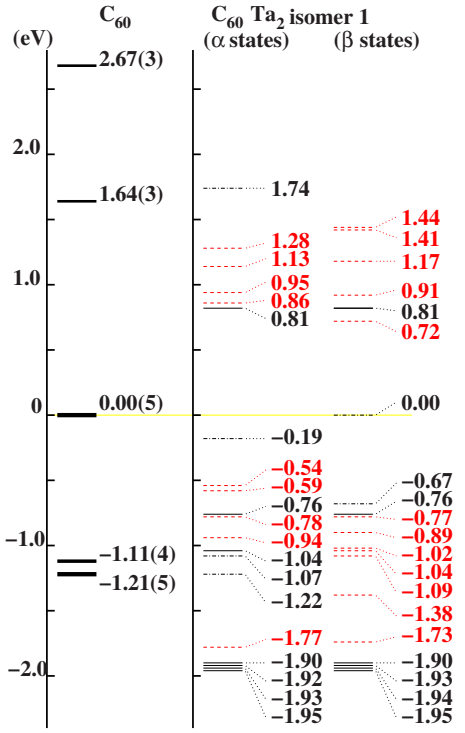

FIG. 4. (Color online) Kohn-Sham eigenvalues close to the band gap for C_{60} and for the most stable isomer of $C_{60}Ta_2$. The numbers in the parentheses denote the degeneracy of the energy levels. Solid and dashed lines indicate levels with a dominant C-like and Ta-like characters, respectively. Dash-dotted lines indicated mixed Ta-C levels.

−1.77 eV are predominantly Ta-like. The reduced number of C-like states within this interval, and the smaller values of the HOMO-LUMO band gap, are indicative of the enhanced reactivity of this heterofullerene not only with respect to C_{60}, but also when compared to $C_{60}Ta$. Figure 5 allows to understand how the different Ta-like, C-like, or Ta-C characters have been assigned. The HOMO-1 level for the α-spin band, located at −0.54 eV in Fig. 4, is found predominantly on one of the Ta atoms. A mixed Ta-C character characterizes the HOMO-1 of the β-spin band, located at −0.67 eV, since pockets of isodensity surfaces can be detected both on the vicinity of one of the two Ta atoms and close to C atoms far from the Ta-C interaction region. For the HOMO levels, the assignments involve sizeable regions encompassing both Ta and C atoms along their bonds with Ta. Finally, the LUMO states are mostly C-like (α, Kohn-Sham energy 0.81 eV) and Ta-like (β, Kohn-Sham energy 0.72 eV), respectively.

Coming to the Kohn-Sham energy levels of the $C_{60}Ta_3$ system (Fig. 6), we notice that a striking difference exists with respect to the case of $C_{60}Ta_2$. Most of the occupied states below the gap are C-like or have a mixed Ta-C character, while the opposite holds above the band gap, meaning that Ta atoms are more likely to play a role in chemical reaction processes involving electronic excited states. Notable exceptions are the HOMO of the β-spin band and an additional eigenstate located 0.52 eV below. A set of Ta like states can be found in the intervals −1.30/−1.51 eV and −1.38/−1.62 eV for the α-spin and β-spin bands, respectively. The corresponding spatial distribution of the HOMO-1, HOMO, and LUMO eigenstates is shown in Fig. 7.

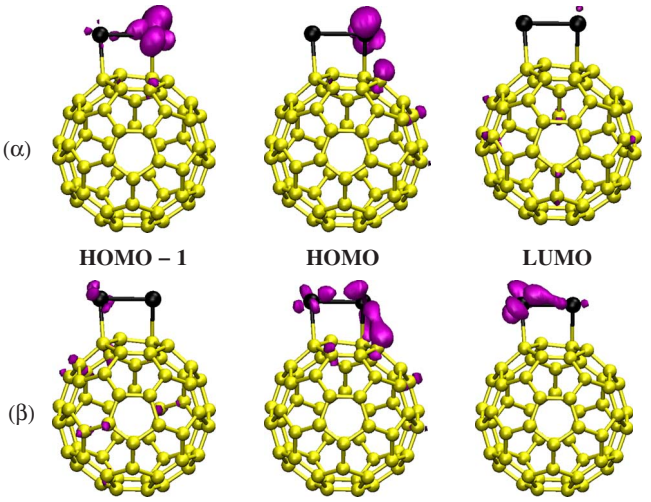

FIG. 5. (Color online) The probability isodensity surfaces, taken at the value 0.005 e/(a.u.)^3, for the eigenstates HOMO-1, HOMO, and LUMO of the most stable isomer of $C_{60}Ta_2$. Top row for the α (minority) spin states and bottom row for the β (majority) spin states.

B. Population analysis and magnetic properties

In terms of Mulliken charges and valence, bonding of Ta atoms to the fullerene results in a charge transfer toward the

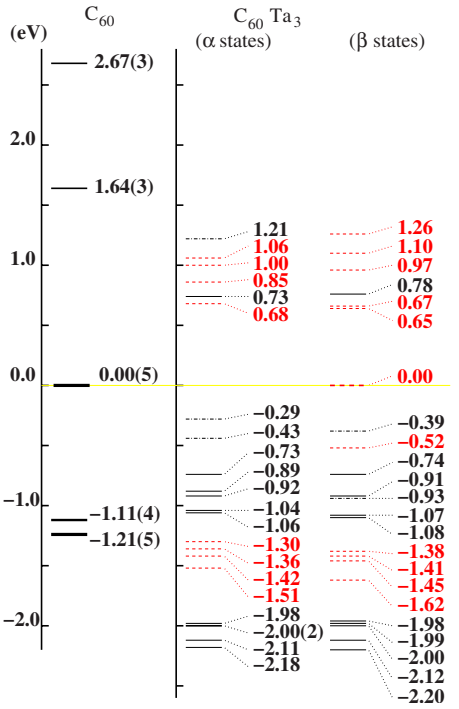

FIG. 6. (Color online) Kohn-Sham eigenvalues close to the band gap for C_{60} and for the most stable isomer of $C_{60}Ta_3$. The numbers in the parentheses denote the degeneracy of the energy levels. Solid and dashed lines indicate levels with a dominant C-like and Ta-like characters, respectively. Dash-dotted lines indicated mixed Ta-C levels.

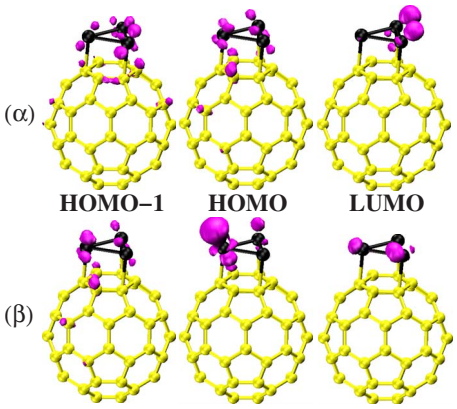

FIG. 7. (Color online) The probability isodensity surfaces, taken at the value 0.005 $e/(a.u.)^3$, for the eigenstates HOMO-1, HOMO, and LUMO of the most stable isomer of $C_{60}Ta_3$. Top row for the α (minority) spin states and bottom row for the β (majority) spin states.

more electronegative C atoms. The values of the positive charges on the Ta atoms range from 1.61 (in $C_{60}Ta_3$) and 1.77 (in $C_{60}Ta_2$) to 2.12 (in $C_{60}Ta$). Neighboring C atoms carry a negative charge amounting to −0.28 (in $C_{60}Ta_2$), while those farther apart from the Ta atoms are essentially neutral (see Table I). The values of the valence on the Ta atoms are indicative of the number of nearest neighbors, since they are found to increase from 1.29 ($C_{60}Ta$, one C nearest neighbor) to 1.96/2.03 ($C_{60}Ta_2$, one C and one Ta nearest neighbors) and then to 3.00/3.25/3.28 in $C_{60}Ta_3$ (two Ta and C nearest neighbors). Based on the Mulliken population analysis and the computed valence charges, no clearcut

TABLE I. Electronic properties of the most stable isomers of $C_{60}Ta$, $C_{60}Ta_2$, and $C_{60}Ta_3$. C′ denotes C atoms which are the nearest neighbors to Ta atom. Spin densities are given in $|e|$ units.

Isomers	Atom	Mulliken charge	Valence	Spin density
$C_{60}Ta$	Ta	2.12	1.29	1.037
	C′	−0.26	3.70	−0.019
	C′	−0.26	3.70	−0.022
	C	0.03–0.04	3.89–3.90	
$C_{60}Ta_2$	Ta	1.77	2.03	−1.467
	Ta	1.80	1.96	1.486
	C′	−0.21	3.70	0.032
	C′	−0.28	3.67	−0.048
	C′	−0.19	3.76	0.048
	C′	−0.27	3.73	−0.028
	C	0.01–0.05	3.87–3.90	−0.03–0.07
$C_{60}Ta_3$	Ta	1.61	3.25	−0.073
	Ta	1.62	3.00	0.870
	Ta	1.61	3.28	−0.077
	C′	−0.22	3.74	−0.03
	C′	−0.21	3.75	0.02
	C′	−0.20	3.76	−0.02
	C	0.03–0.04	3.75–3.90	−0.02–0.05

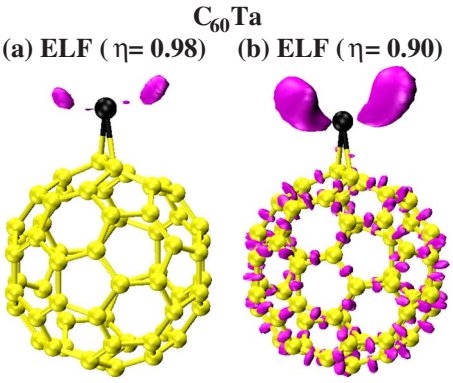

FIG. 8. (Color online) ELF for $C_{60}Ta$. (a) Four basins are visible around Ta site at η=0.98. (b) These basins are merged into two major localization regions at η=0.90.

indication can be found about the nature of the bonding between the dopant species and the fullerene cage. In particular, the role of charge transfer in establishing the bonding character remains to be elucidated. The electron localization properties presented in the next section turned out to be very well suited to achieve this purpose.

Spin-density values given in Table I are those corresponding to the lowest multiplicity spin states for each one of the three clusters. We have checked that this choice does correspond to the lowest energy when compared to other spin configurations. Common to the three cases is the presence of a predominant spin density on the Ta atoms, much smaller, albeit non-negligible, spin densities being found on the neighboring C atoms. $C_{60}Ta_2$ features a singlet state with two spin densities of opposite signs on the Ta atoms. Instead of being delocalized on the three Ta atoms, a much larger spin density is found on one of the Ta atoms in $C_{60}Ta_3$. Vanishing spin densities characterize the C atoms lying far from the Ta impurities. Taken altogether, these results demonstrate that the Ta atoms are the only responsible for the magnetic nature of these clusters, whereas the C atoms are barely affected.

C. Electron localization function and localized orbitals

An analysis of the electron localization regions in the Ta-C_{60} systems was performed in terms of the ELF and visualized in terms of three-dimensional isosurfaces, as shown in Fig. 8. By decreasing the ELF values, four localization basins appear, visible around the Ta site on both sides of the ideal plane formed by Ta and the two C atoms connected by the $h-h$ bond. These basins merge in two major localization regions at η=0.9, while further localization basins appear in the region of the Ta-C bonds and in the regions between all the C-C bonds in the C_{60} structure. The domains along the Ta-C bonds are shifted toward the C atoms to indicate a polar character in the C-Ta bonding. The existence of a localization region located in the vicinity of the doping atom but clearly separated from the bonds with C atoms is analogous to a situation already encountered in the case of $C_{59}Si$.[29,30] In that case, such a region could be ascribed to the sp^2 "weak" bonding of Si in the C_{60} environment, leaving nonbonded one valence electron for Si atom. In the present case, it ap-

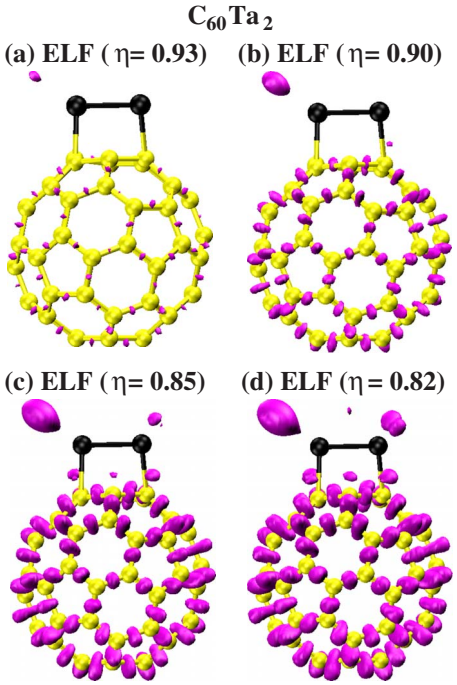

FIG. 9. (Color online) ELF for $C_{60}Ta_2$. Note that the localization region external to the Ta atom appears already at η=0.93, while those corresponding to Ta-C bonds are visible on both bonds at η=0.85.

pears that the five valence electrons of Ta contribute to two distinct localization patterns in the ELF. The first is highly localized (smaller Pauli repulsion among electrons, as based on the ELF definition), while the second is related to the fraction of the valence electron density more spread out in space since it is involved in bonds with C atoms.

A similar pattern can be observed in the ELF behavior of $C_{60}Ta_2$, a few differences being noticeable (Fig. 9). First, the localization region external to the Ta atom farther apart from the cage appears at (η=0.93), along with the localization basins located on each C-C bond. At lower values (η =0.90), the ELF regions are visible around the C atom bound to one of the Ta atoms and then (η=0.85) along both Ta-C bonds. Interestingly, the localization regions pertaining to the Ta-Ta bond become visible at lower ELF values (above the bond, η=0.82), suggesting that a higher Pauli repulsion is effective, due to *d* electrons. Overall, it appears that the external doping of C_{60} by Ta has the effect of localizing the valence electron density not only along the Ta-C bond but also, and more predominantly, on regions of space surrounding the Ta atom. For $C_{60}Ta$ and $C_{60}Ta_2$, these regions correspond to the Ta valence electrons not involved in bond formation.

The global information about the electron localization provided by the ELF can be partitioned into single-orbital contributions by means of the maximally localized WF and WFC analyses, as shown for a variety of systems ranging from solids to liquids.[31–33] By this approach, we see that three of these centers, labeled as WFC1, WFC2, and WFC3 in Fig. 10, are distributed around the Ta atoms. The remaining two, labeled as WFC4 and WFC5, are located along the Ta–C bonds [Fig. 10(a)]. Therefore, three of the five Ta va-

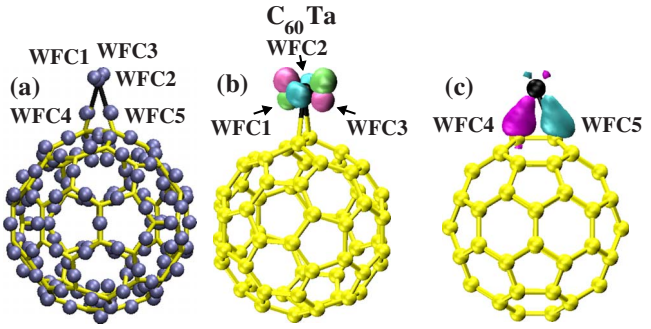

FIG. 10. (Color online) (a) Wannier function centers around Ta site. Three centers around Ta atom are labeled as WFC1, WFC2, and WFC3, respectively. The remaining two, which are located along the Ta-C bonds, are labeled as WFC4 and WFC5, respectively. (b) Maximally localized Wannier functions for WFC1, WFC2, and WFC3 plotted at a value 0.02 $[e/(a.u.)^3]$. (c) The same for WFC4 and WFC5, which take part in the formation of the Ta-C bonds.

lence electrons do not participate in the formation of Ta-C bonds but remain localized around the Ta site. Conversely, two valence electrons take part in the formation of the Ta-C bonds, as shown in panels (b) and (c) of Fig. 10. The isosurfaces, plotted at a value of 0.02 $e/(a.u.)^3$, refer to the Wannier functions of the states WFC1, WFC2, and WFC3 [panel (b)], and WFC4 and WFC5 [panel (c)]. The largest amplitudes of WFC4 and WFC5 are shifted toward the C atoms of the C_{60}, conferring a peculiar "pear" shape to these electronic distributions and underscoring the fact that the Ta-C bond has a polar character. These pieces of evidence substantiate the view of a charge transfer from the Ta atom favoring bond formation in the direction of the C atoms, thereby conferring to the Ta-C interactions a nontrivial ionocovalent character.

In Fig. 11, we show the Wannier centers of $C_{60}Ta_2$. By attributing ten of them to the presence of Ta atoms, one can distinguish four centers located on the Ta atoms (two on each) and other two centers in the region between the Ta-C bonds. These six centers are not related to bond formation involving either the Ta pair of atoms or any neighboring C atom. Among the remaining four WFCs, two are found along the Ta-Ta bond and the last two along the Ta-C bonds (one of each bond). The corresponding WFs are shown in Fig. 12. It appears that four WFs are strictly localized on each of the Ta atoms [Fig. 12(a)], as expected in view of the existence of the two corresponding WFCs. Similarly, two WFs are spread out in the space between the bonds [Fig. 12(b)]. Finally, two Wannier functions are indicative of Ta-Ta and Ta-C bond formations, respectively, thereby confirming the picture of the Ta atom behaving in $C_{60}Ta_2$ as a divalent impurity [Fig. 12(c)].

Based on these observations, the transition from the divalent behavior of Ta observed in $C_{60}Ta_2$ to the trivalent behavior of Ta expected in $C_{60}Ta_3$ can be rationalized as follows. One can attribute the 15 Wannier centers stemming from the presence of three Ta impurities to specific bonds and/or locations. We begin with the consideration that each Ta-Ta bond accounts for two Wannier centers (one for each

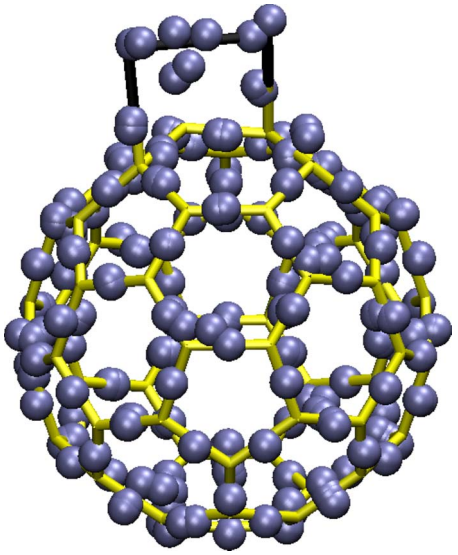

FIG. 11. (Color online) Wannier centers for $C_{60}Ta_2$. We attribute ten of them to the presence of the Ta atoms, namely, the eight visible on the top of the figure in the vicinity of the Ta atoms and one of each of the Ta-C bonds.

Ta, see above) and each Ta-C bond for one Wannier center. Therefore, we have as much as nine Wannier centers pertaining to Ta atoms, i.e., nine valence electrons are involved in bonding formation and six are localized on Ta atoms. This picture is consistent both with the values found for the valence in $C_{60}Ta_3$ and with the charge on the Ta atoms (smaller in $C_{60}Ta_3$ than in $C_{60}Ta_2$ and $C_{60}Ta$). Indeed, the formation of Ta-Ta bonds induces electron density delocalization out of the Ta ionic centers, lowering the charge on these atomic sites.

IV. CONCLUSIONS

We have performed an analysis of the electronic properties of $C_{60}Ta$, $C_{60}Ta_2$, and $C_{60}Ta_3$ by focusing on the most stable isomers for each of the three heterofullerenes. The perturbation induced by the dopant Ta atoms is reflected by radical changes around the HOMO and LUMO Kohn-Sham levels. This is particularly striking in the case of $C_{60}Ta_2$, the formation of a Ta_2 dimer resulting in a predominant presence of Ta-like states within an energy range of ~3.5 eV around the HOMO level. There are profound differences between the Kohn-Sham levels of $C_{60}Ta$ and those of an unperturbed C_{60}+Ta isomer obtained without relaxing the atomic positions. In this latter system, Ta-like and C-like states lie almost entirely in separated portions of the energy band. Mulliken charges indicate a charge transfer of approximately two e^- toward the C_{60}, in all the three cases, increasing from 1.61 ($C_{60}Ta_3$) to 2.12 ($C_{60}Ta$). The nominal Ta valence reflects the coordination of the dopant atoms, being close to 1, 2, and 3 for $C_{60}Ta$, $C_{60}Ta_2$, and $C_{60}Ta_3$, respectively.

We employ the electron localization function ELF and the Wannier functions approach to better characterize Ta-Ta and Ta-C bonding in the case of $C_{60}Ta$ and $C_{60}Ta_2$. Charge transfer to the C atoms has to be interpreted as a delocalization of

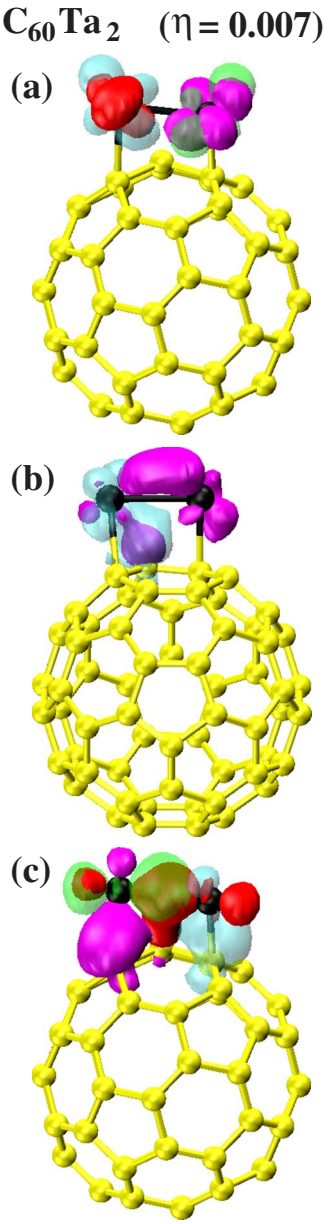

FIG. 12. (Color online) Maximally localized Wannier functions for $C_{60}Ta_2$ plotted at a value of 0.007 e/(a.u.)^3. These Wannier functions are those corresponding to the Wannier centers shown in Fig. 9. (a) A total of four Wannier functions, i.e., two pairs localized at each one of the Ta locations. (b) Two Wannier functions spatially distributed in between the Ta-C bonds and the Ta-Ta bond. (c) Four Wannier functions localized along the Ta-Ta bond (two of them) and the Ta-C bonds (one on each bond).

Ta valence electrons (no more than two) in the direction of the nearest neighbors, while the remaining valence electrons of each Ta remain close to the Ta site. This picture is confirmed by the location and spread of the WFCs. Three WFs are located on the Ta atom in $C_{60}Ta$ and are not involved in the bonding. Similarly, in the case of $C_{60}Ta_2$, only four WFs (two for each Ta atom) are distributed along Ta-Ta or Ta-C bonds. As a natural extension of these findings, bonding in $C_{60}Ta_3$ results from the involvement of three valence

electrons for each Ta atom, responsible for two Ta-Ta and one Ta-C bonds, respectively. Therefore, our calculations are instrumental to identify a change in the valence state with increasing number of Ta atoms.

The present results show that the interactions in the neighborhood of the dopant sites consist of covalent bonds between Ta atoms and by ionocovalent bonds between Ta and C atoms. In all case studied, charge transfer is responsible for the formation of both nonzero electron densities located between Ta and C atoms and Ta-Ta bonds. In Ref. 13, first-principle molecular dynamics showed that the fragmentation behavior of these systems is not consistent with the emission of C_n units, at least on the picosecond time scale. In this paper, we showed that there is clear physical mechanism underlying the formation of small Ta units adsorbed on the C_{60} cage, at least when local equilibrium structural and ground-state electronic properties are taken into account. Therefore, our results suggest that any experimental observation of C_n units might result from processes not included in the present framework, i.e., electronic excitation.

[1] P. Mélinon, B. Masenelli, F. Tournus, and A. Perez, Nature Mater. **6**, 479 (2007).
[2] O. Vostrowsky and A. Hirsch, Chem. Rev. **106**, 5191 (2006).
[3] W. Andreoni, Annu. Rev. Phys. Chem. **49**, 405 (1998).
[4] I. M. L. Billas, C. Massobrio, M. Boero, M. Parrinello, W. Branz, F. Tast, N. Malinowski, M. Heinebrodt, and T. P. Martin, Comput. Mater. Sci. **17**, 191 (2000).
[5] M. M. G. Alemany, O. Diéguez, C. Rey, and L. J. Gallego, J. Chem. Phys. **114**, 9371 (2001).
[6] Q. Kong, Y. Shen, L. Zhao, J. Zhuang, S. Qian, Y. Li, Y. Lin, and R. Cai, J. Chem. Phys. **116**, 128 (2002).
[7] Q. Kong, J. Zhuang, J. Xu, Y. Shen, Y. Li, and L. Zhao, J. Phys. Chem. A **107**, 3670 (2003).
[8] J. M. Campanera, C. Bo, A. L. Balch, J. Ferré, and J. M. Poblet, Chem.-Eur. J. **11**, 2730 (2005).
[9] O. Loboda, V. R. Jensen, and K. J. Børve, Fullerenes, Nanotubes, Carbon Nanostruct. **14**, 365 (2006).
[10] M. Sparta, K. J. Børve, and V. R. Jensen, J. Phys. Chem. A **110**, 11711 (2006).
[11] M. Sparta, V. R. Jensen, and K. J. Børve, Fullerenes, Nanotubes, Carbon Nanostruct. **14**, 269 (2006).
[12] C. Tang, K. Deng, W. Tan, Y. Yuan, Y. Liu, J. Yang, and X. Wang, Eur. Phys. J. D **43**, 125 (2007).
[13] L. M. Ramaniah, M. Boero, and M. Laghate, Phys. Rev. B **70**, 035411 (2004).
[14] F. Tast, N. Malinowski, S. Frank, M. Heinebrodt, I. M. L. Billas, and T. P. Martin, Phys. Rev. Lett. **77**, 3529 (1996).
[15] R. Car and M. Parrinello, Phys. Rev. Lett. **55**, 2471 (1985).
[16] CPMD, Copyright IBM Corp (1990–2008) and MPI für Festkörperforschung Stuttgart (1997–2001) (1990–2008), http://www.cpmd.org/
[17] A. D. Becke, Phys. Rev. A **38**, 3098 (1988).
[18] C. Lee, W. Yang, and R. G. Parr, Phys. Rev. B **37**, 785 (1988).
[19] N. Troullier and J. L. Martins, Phys. Rev. B **43**, 1993 (1991).
[20] A. D. Becke and K. E. Edgecombe, J. Chem. Phys. **92**, 5397 (1990).
[21] A. Savin, A. D. Becke, J. Flad, R. Nesper, H. Preuss, and H. G. von Schnering, Angew. Chem., Int. Ed. Engl. **30**, 409 (1991).
[22] A. Savin, O. Jepsen, J. Flad, O. K. Andersen, H. Preuss, and H. G. von Schnering, Angew. Chem., Int. Ed. Engl. **31**, 187 (1992).
[23] A. Savin, R. Nesper, S. Wengert, and T. F. Fässler, Angew. Chem., Int. Ed. Engl. **36**, 1808 (1997).
[24] S. F. Boys, *Localized Orbitals and Localized Adjustment Functions* (Academic Press, New York, 1966), p. 253.
[25] G. H. Wannier, Phys. Rev. **52**, 191 (1937).
[26] N. Marzari and D. Vanderbilt, Phys. Rev. B **56**, 12847 (1997).
[27] M. Matsubara and C. Massobrio, J. Phys. Chem. A **109**, 4415 (2005).
[28] M. Matsubara and C. Massobrio, J. Chem. Phys. **122**, 084304 (2005).
[29] I. M. L. Billas, F. Tast, W. Branz, N. Malinowski, M. Heinebrodt, T. P. Martin, C. Massobrio, M. Boero, and M. Parrinello, Eur. Phys. J. D **9**, 337 (1999).
[30] I. M. L. Billas, C. Massobrio, M. Boero, M. Parrinello, W. Branz, F. Tast, N. Malinowski, M. Heinebrodt, and T. P. Martin, J. Chem. Phys. **111**, 6787 (1999).
[31] P. L. Silvestrelli, N. Marzari, D. Vanderbilt, and M. Parrinello, Solid State Commun. **107**, 7 (1998).
[32] P. L. Silvestrelli and M. Parrinello, Phys. Rev. Lett. **82**, 3308 (1999).
[33] M. Boero, J. Phys. Chem. A **111**, 12248 (2007).